SANDIA REPORT
SAND2019-0924
Printed Click to enter a date

Sandia National Laboratories

Near-Field Imaging of Shallow Chemical Detonations in Granite using Change Detection Methods of Borehole Seismic Data

Paul C. Schwering, Charles R. Hoots, Hunter A. Knox, Robert E. Abbott, and Leiph A. Preston

Prepared by
Sandia National Laboratories
Albuquerque, New Mexico
87185 and Livermore,
California 94550

Issued by Sandia National Laboratories, operated for the United States Department of Energy by National Technology & Engineering Solutions of Sandia, LLC.

Available to DOE and DOE contractors from
U.S. Department of Energy
Office of Scientific and Technical Information
P.O. Box 62
Oak Ridge, TN 37831

Telephone: (865) 576-8401
Facsimile: (865) 576-5728
E-Mail: reports@osti.gov
Online ordering: http://www.osti.gov/scitech

Available to the public from
U.S. Department of Commerce
National Technical Information Service
5301 Shawnee Rd
Alexandria, VA 22312

Telephone: (800) 553-6847
Facsimile: (703) 605-6900
E-Mail: orders@ntis.gov
Online order: https://classic.ntis.gov/help/order-methods/

ABSTRACT

As part of the Source Physics Experiment (SPE) Phase I shallow chemical detonation series, multiple surface and borehole active-source seismic campaigns were executed to perform high-resolution imaging of seismic velocity changes in the granitic substrate. Cross-correlation data processing methods were implemented to efficiently and robustly perform semi-automated change detection of first-arrival times between campaigns. The change detection algorithm updates the arrival times, and consequently the velocity model, of each campaign. The resulting tomographic imagery reveals the evolution of the subsurface velocity structure as the detonations progressed.

ACKNOWLEDGEMENTS

The authors thank Dan Herold, Bob White, Kale McLin, Ryan Emmit, Maggie Townsend, Curtis Obi, Fred Helsel, Rebekah Lee, Liam Toney, Matt Geuss, and Josh Feldman for their direct and invaluable contributions to this work.

Sandia National Laboratories is a multi-mission laboratory managed and operated by National Technology & Engineering Solutions of Sandia, LLC, a wholly owned subsidiary of Honeywell International Inc., for the U.S. Department of Energy's National Nuclear Security Administration under contract DE-NA0003525.

This paper describes objective technical results and analysis. Any subjective views or opinions that might be expressed in the paper do not necessarily represent the views of the U.S. Department of Energy or the United States Government. Note that a more detailed manuscript for this work is being prepared for publication in the Bulletin of the Seismological Society of America (BSSA).

CONTENTS

LIST OF FIGURES

LIST OF TABLES

This page left blank

ACRONYMS AND DEFINITIONS

Abbreviation	Definition
AWD	accelerated weight drop
CBCD	cross-borehole change detection
CC	cross-correlation coefficient
EMP	electromagnetic pulse
m/s	meters per second
NNSS	Nevada National Security Site
P-wave	compressional wave
SNR	signal-to-noise ratio
SPE	Source Physics Experiment
t_0	trigger time, zero-time
Vp	P-wave velocity

1. INTRODUCTION

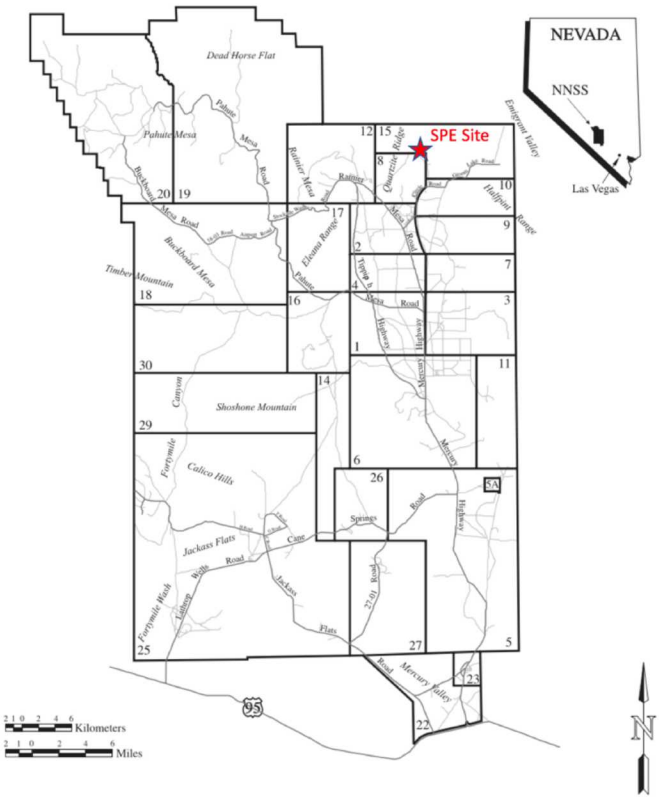

The first SPE (Source Physics Experiment) phase comprises a series of shallow (< 100 meters below ground surface) chemical detonations performed in a single borehole at a hard rock site located in the Nevada National Security Site (NNSS; see inset site location map at left*). The host geology is Climax Stock granite that is weathered within approximately 40 meters of the ground surface, transitioning to competent rock below the weathered zone (Townsend et al., 2012). Groundwater was encountered approximately 20 to 25 meters below ground level at the site (Townsend and Obi, 2015).

Water level monitoring boreholes (Figure 2-1) were drilled within a 50-meter radius of the detonation borehole, enabling near-field cross-borehole seismic tomographic imaging of compressional (P-) wave velocity in the hard rock subsurface (e.g., Lines and LaFehr, 1989 and Cao and Greenhalgh, 1997). The primary objective of this study was to perform a series of active-source, cross-borehole change detection (CBCD) seismic campaigns to image velocity changes in the subsurface during the SPE Phase I detonation series. Surface seismic refraction data added to the near-surface tomographic constraints. Cross-correlation data processing methods similar to those used for earthquake (e.g., Schaff et al., 2004) and ambient noise (e.g., Meier et al., 2010) seismology were leveraged to meet the objective.

* *Map adapted from figure in DOE/OSTI document DOE/NV--1462.*

2. DATA ACQUISITION

For each CBCD campaign, data were collected in and between boreholes "BH-009" and "BH-189", coplanar with the explosives emplacement borehole "GZ" (Figure 2-1). The surface source was an accelerated weight drop (AWD), recorded by 24 geophones on the ground surface spanning the two boreholes. A plasma seismic source ("sparker") and a 24-channel string of hydrophones were utilized in the two monitoring boreholes. When accessible, the GZ borehole was instrumented with hydrophones as well. One-second records were acquired at a 0.0625 millisecond sample interval, with a 10 ms trigger delay.

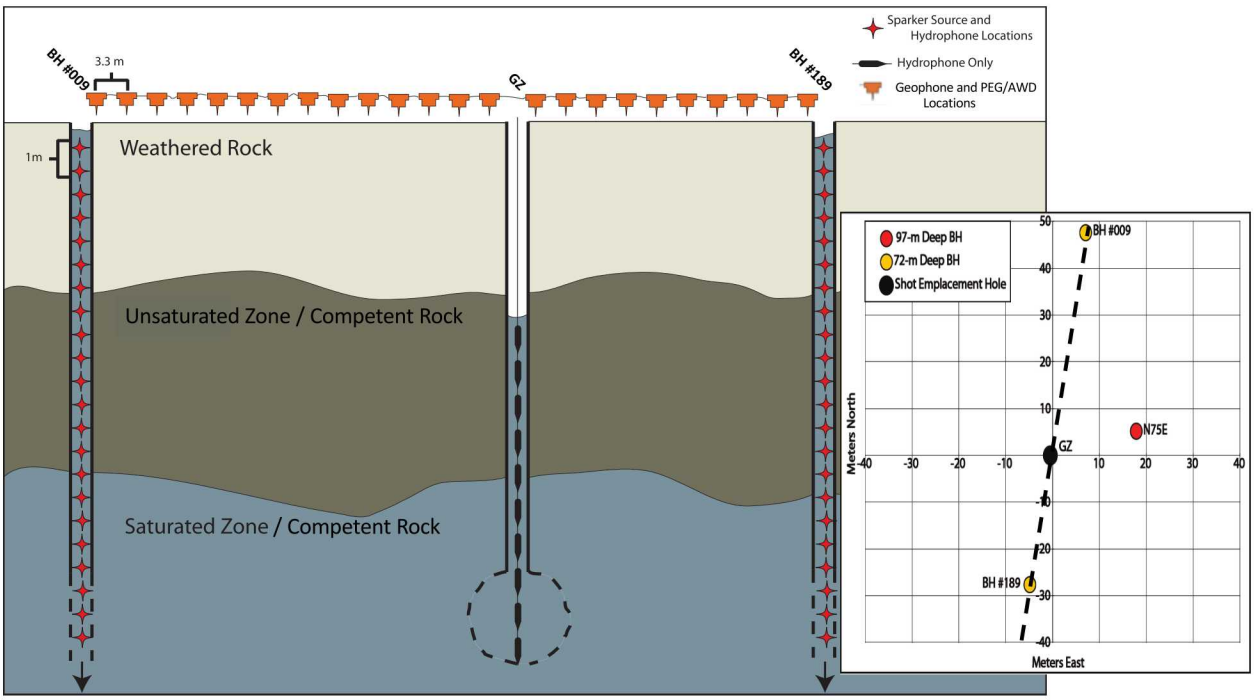

Figure 2-1. Cross-section schematic of CBCD source/receiver layout for seismic data acquisition (not to scale); inset shows to-scale map view of cross-section location (black, dashed line). Hydrogeologic layering shown here for illustrative purposes, not on a quantitative basis.

Sparker shots were performed at 1-meter depth increments in the two monitoring wells, with the hydrophone string (1-meter channel interval) occupying the opposing borehole or GZ. The sequence of SPE detonations and CBCD deployments are outlined in Table 1. Note that differing source/receiver occupations among the CBCD phases were typically a result of changing borehole conditions (e.g., GZ was not accessible during CBCD-3).

Table 2-1. Timing and details of SPE detonation and CBCD deployment phases.

Date (mo. & yr.)		**Phase**	**SPE Depth** (m)	**SPE Yield** (kg TNT)	**CBCD Source Deployments**	**CBCD Receiver Deployments**
May 2011		SPE-1	55.1	90	-	-
Oct 2011		SPE-2	45.7	997	-	-
Jun 2012		CBCD-1	-	-	BH #009 BH #189 AWD	BH #009 BH #189 GZ Geophones
Jul 2012		SPE-3	47.2	905	-	-
Jul 2012		CBCD-2	-	-	Incomplete	Incomplete
Aug 2012		CBCD-3	-	-	BH #009 BH #189 AWD	BH #009 BH #189 Geophones
Nov 2013		SPE-4	Incomplete	Incomplete	-	-
Feb 2015		CBCD-4	-	-	BH #009 BH #189 AWD	BH #009 BH #189 GZ Geophones
May 2015		SPE-4p	87.2	89	-	-
Apr 2016		SPE-5	76.5	5,035	-	-
Jul 2016		CBCD-5	-	-	BH #009 BH #189 GZ AWD	BH #009 BH #189 Geophones
Oct 2016		SPE-6	31.4	2,245	BH #009 BH #189 AWD	BH #009 BH #189 Geophones

3. DATA PROCESSING

Following data collection, the field records were processed and reviewed for signal quality (Figure 3-1). Surface refraction and cross-borehole data sets were of good quality overall, though signal-to-noise ratio (SNR) varied. Poor quality data records were removed from further analysis. Typically, less than 5% of each CBCD data set were removed, with the exception of CBCD-6 (Table 2).

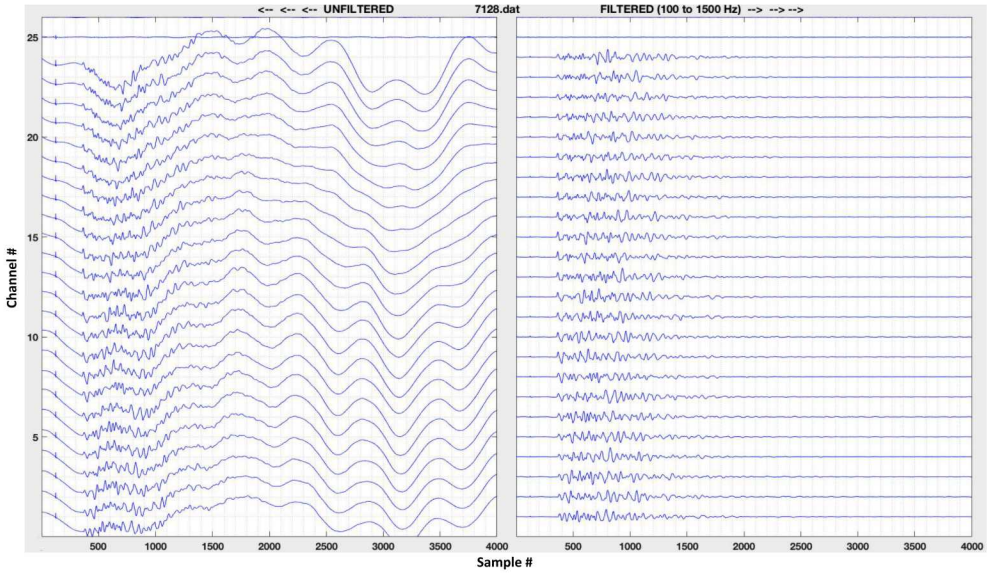

Figure 3-1. At left, raw traces from field file '7128.dat', a 24-channel cross-borehole shot gather from CBCD-5 (sparker in BH #009, hydrophones in BH #189). At right, same shot gather filtered for analysis (Butterworth bandpass filter from 100 to 1,500 Hz). Note removal of high-amplitude, low-frequency oscillations attributed to water column motion in receiver borehole.

Table 3-1. Percentages of removed cross-borehole data files from each CBCD phase.

Phase	CBCD-1	CBCD-3	CBCD-4	CBCD-5	CBCD-6
Removed File Percentage	2.0%	4.4%	4.8%	3.7%	11.6%

Closer examination of the cross-borehole traces revealed timing errors in the data. These timing errors were caused by inconsistent triggering of the data recorder. To enhance the SNR of the records, several (typically 3 to 10) records were collected for each shot location and then stacked. The raw, unstacked data revealed a high-frequency pulse that accompanied each shot trigger well before the seismic arrival. This phenomenon was traced to an electromagnetic pulse (EMP) that resulted from the nearly instantaneous discharge of 5,000 kilovolts of electricity from the control box coupling into the borehole string. The cable connecting the downhole hydrophone array to the data recorder at the surface effectively became an electromagnetic antenna. The advantage of identifying this effect is that the EMP pulse provided a precise trigger, or zero-time (t_0), for each record. Examination of individual stacks revealed that the EMP signals were not always consistent from source to source (e.g., Figure 3-2), indicating triggering errors that merit prestack signal conditioning (e.g., Singleton, 2009).

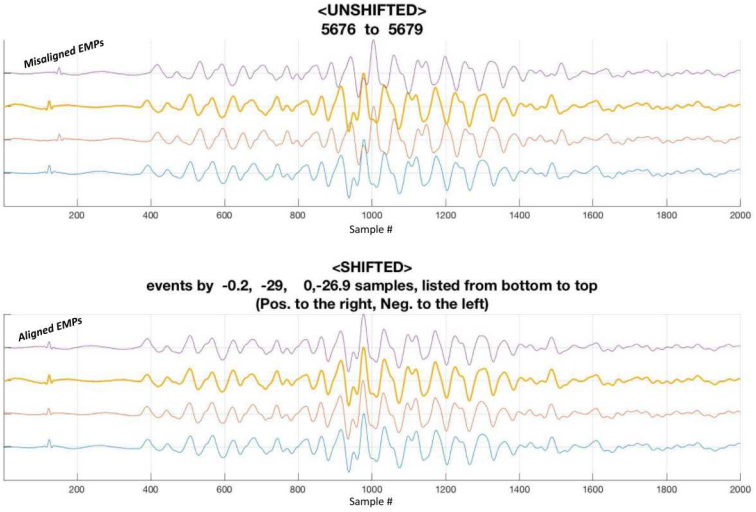

Figure 3-2. At top, traces from source gathers (same source & receiver pairs) from CBCD-4 that are misaligned due to timing errors. At bottom, same traces shifted to align EMP.

Fortunately, the accuracy and precision of the recorded EMP signals allowed for prestack correction of the timing errors. We developed a cross-correlation algorithm that took advantage of the consistency of the EMP signals in order to shift misaligned stacks into alignment (Figure 3-2). This proved in some cases to be an important correction, as stacking of misaligned records resulted in poorly stacked data (e.g., Figure 3-3) due to deconstructive interference. In some cases, the impulsiveness of the first-arriving energy was significantly reduced, which can have significant adverse consequences when picking phases in a high-velocity, short-offset geometry (e.g., Singleton, 2009). By systematically identifying timing errors in prestack data and aligning the records, the SNR and confidence of the stacked records were preserved (Figure 3-3).

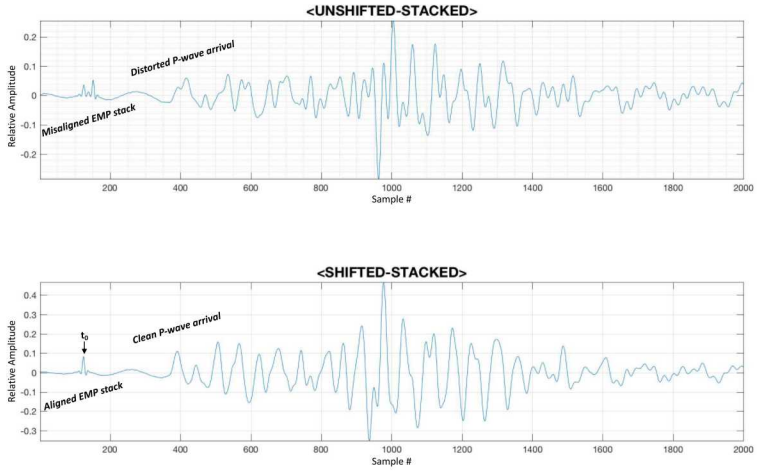

Figure 3-3. At top, stacked data trace from CBCD-4 showing results of stacking traces with timing errors. At bottom, same trace stack showing results of timing correction in which the aligned EMP peak is then assigned as t_0 for the stacked shot record.

Following manual picking of P-wave first arrivals from CBCD-1, change detection was performed using a cross-correlation algorithm on subsequent data sets. P-wave first arrivals of CBCD-1 were picked by an analyst to establish CBCD-1 as the 'baseline' data set for change detection. Cross-correlation of data sets was then implemented phase-by-phase; i.e., CBCD-1 ★ CBCD-3, CBCD-3 ★ CBCD-4, … CBCD-n ★ CBCD-n+1. The cross-correlation method at a trace-by-trace scale essentially uses P-wave first break pick times of the previous data set as a time window reference for cross-correlation with the subsequent data set. Using a similar approach to that described by Schaff et al. (2004), the algorithm computed the maximum cross-correlation coefficient (CC) for each trace within the time-window range and shifted the subsequent trace by the associated time (e.g., Figure 3-4). Data with normalized CC values of less than 0.75 were removed from further analysis. For the remaining data, the magnitude of the time shift that resulted in a maximum cross-correlation coefficient value was used to identify the new pick time. That is, for a given pair of traces from one 'known' data set and one 'unknown' data set:

$$T_n + \Delta t_\star = t_{n+1},$$

where t_n is the P-wave first arrival pick time from the 'known' trace, $\Delta t_\star$ is the optimized cross-correlation time shift, and t_{n+1} is the P-wave first arrival time assigned to the 'unknown' trace. This algorithmic approach allows for more efficient, accurate, and consistent change detection than manual picking.

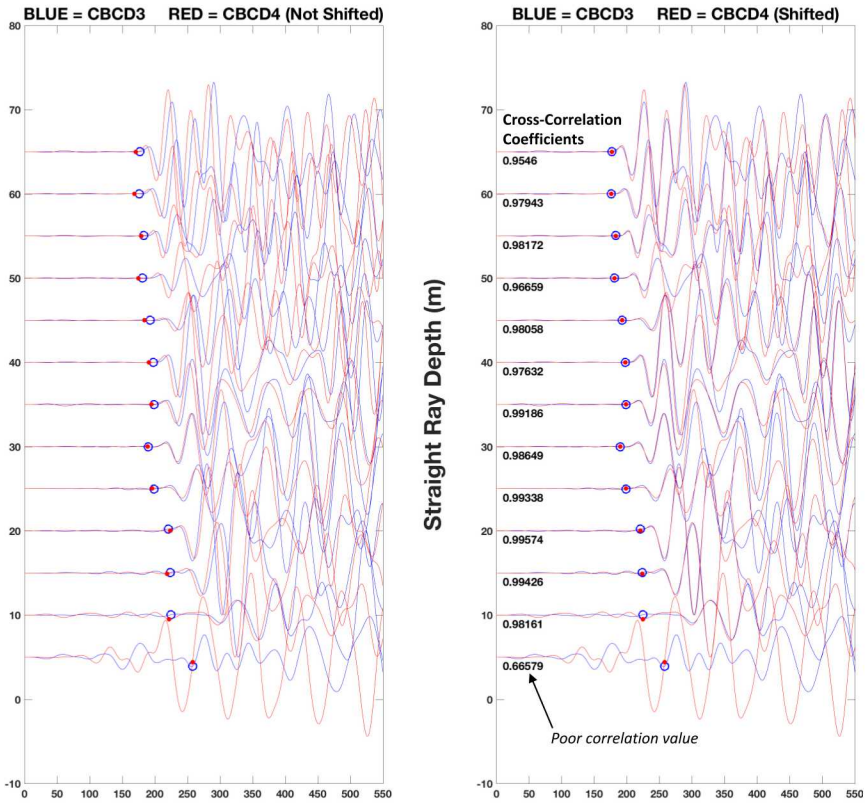

Figure 3-4. Before (left) and after (right) alignment of traces based on cross-correlation of CBCD-4 with CBCD-3. Note that straight ray traces (i.e., source and receiver at equal depths) are used here for ease of comparison, and that traces have been shifted to t_0 (horizontal axis = sample #).

4. TOMOGRPAHIC INVERSION

P-wave velocity (Vp) tomographic models were produced for each CBCD phase (Figure 4-1). The data were inverted using Tomog – an internal Sandia tomography code that exploits a ray-based (eikonal) P-wave travel-time tomographic inversion methodology (Preston, 2009). Input P-wave travel times are weighted by estimated error, and uniform error is assumed (i.e., equal weighting on all observations). Model parameters are continuously evaluated up to a pre-defined set of convergence criteria through an iterative inverse procedure using incremental changes in model parameters based on travel-time residuals (i.e., observed minus calculated). After model convergence criteria are met, the final Vp tomogram is produced in units of meters per second (m/s). 2D Vp models are displayed with ray path coverage models for comparison (Figure 4-1).

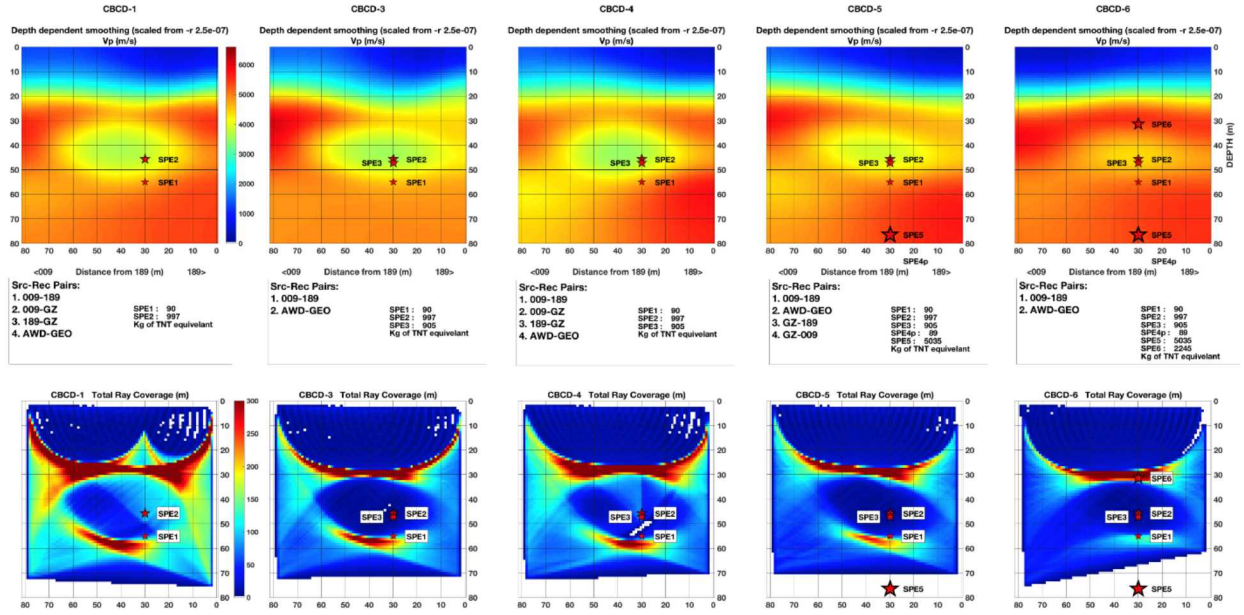

Figure 4-1. Top, 2D models of Vp inversion tomograms for each of the CBCD phases overlain with locations of prior SPE detonations. Details of the CBCD deployments and SPE detonations are also provided below each Vp model; refer to Table 1 for further details. Bottom, 2D models of P-wave ray coverage for each of the CBCD phases. For all models, the vertical trace of BH #009 forms the left extent (82 meters on horizontal axis) and the vertical trace of BH #189 forms the right extent (0 meters on horizontal axis); see also Figure 2-1. The vertical axis, depth, is referenced to the ground surface (0 meters).

5. DISCUSSION OF RESULTS

The Vp tomograms (Figure 4-1) consistently show increasing seismic velocity with depth. The rate of velocity increase with depth is dramatically reduced approximately 20 to 30 meters below the surface. This transition zone is consistent with groundwater depths at the site (Townsend and Obi, 2015). However, it is not clear how much of an influence the transition from weathered to competent granite (Townsend et al., 2012) may also be contributing to the Vp results.

The primary feature of interest captured in the Vp tomograms is an ellipsoidal low-velocity (Vp < ~4,000 m/s) anomaly near GZ. This is interpreted to be related to the damage that appears to have originated from the SPE-2 detonation. The corresponding ray coverage models indicate that the rays generally avoid this low-velocity zone and instead refract into the surrounding high-velocity rock per Fermat's principle (e.g., Lines and LaFehr, 1989). Interestingly, the size and velocity contrast of this feature diminish significantly after SPE-5 (CBCD-5), and again after SPE-6 (CBCD-6). It appears that these detonations below and then above the SPE-2 damage zone significantly reduced its velocity contrast compared to the surrounding rock.

CBCD-6 results, after the relatively large-yield and shallow-depth SPE-6 detonation, merit further attention. Firstly, the magnitude and depth of SPE-6 may have had a broad impact on CBCD-6 data quality given the higher percentage of data removal compared to the other CBCD phases (Table 2). Regardless, the ray coverage for CBCD-6 appears sufficient for imaging (Figure 4-1). An intuitive expectation for CBCD-6 would be a low-velocity damage zone around SPE-6, similar and perhaps complementary to the one associated with SPE-2. Instead, the primary observable change is a high-velocity 'bulge' above SPE-6, which correlates with on-site observations that the ground surface was uplifted after this detonation. In contrast to SPE-2, it appears that significant explosive energy from SPE-6 was transmitted towards the ground surface and perhaps into the existing damage zone from SPE-2. This inferred redirection of energy may have resulted in decreased energy availability to significantly damage the rock mass surrounding SPE-6.

6. CONCLUSIONS

The CBCD campaign series was successful in its primary objective of detecting and mapping post-detonation changes of active-source seismic signatures in a hard rock environment. In pursuit of this objective, several seismic techniques were developed and implemented. The field methods that were executed enabled collection of high-quality data using relatively low-cost, commercial-grade equipment. A robust methodology was designed for precisely identifying the trigger time (t_0) of data records and employing a reliable and efficient cross-correlation algorithm to remove timing errors prior to data stacking. The cross-correlation technique that was employed, in conjunction with state-of-the-art tomographic inversion, proved efficacious in detection and imaging of near-field, active-source seismic signal changes after chemical detonations.

REFERENCES

[1] Cao, S. and S. Greenhalgh (1997). Cross-well seismic tomographic delineation of mineralization in a hard-rock environment, *Geophys. Prospect.*, **45**, 449-460.

[2] Lines, L. R. and E. D. LaFehr (1989). Tomographic modeling of a cross-borehole data set, *Geophysics* **54**, no. 10, 1249-1257.

[3] Meier, U., N. M. Shapiro, and F. Brenguier (2010). Detecting seasonal variations in seismic velocities within Los Angeles basin from correlations of ambient seismic noise, *Geophys. J. Int.* **181**, 985-996.

[4] Preston, L. (2009). Tomog User Manual, *Technical Paper SAND2009-3082 P*, Sandia National Laboratories, Albuquerque, NM, 21 p.

[5] Schaff, D. P., G. H. R. Bokelmann, W. L. Ellsworth, E. Zanzerkia, F. Waldhauser, and G. C. Beroza (2004). Optimizing correlation techniques for improved earthquake location, *Bull. Seism. Soc. Am.* **94**, 705–721.

[6] Singleton, S. (2009). The effects of seismic data conditioning on prestack simultaneous impedance inversion, *The Leading Edge*, **28 (7)**, 772-781.

[7] Townsend, M. and C. Obi (2015). Data Release Report for Source Physics Experiments 2 and 3 (SPE-2 and SPE-3), Nevada National Security Site, *Technical Report DOE/NV/25946--2282-REV 1*, National Security Technologies, LLC, Las Vegas, Nevada, 442 p.

[8] Townsend, M., L. Prothro, and C. Obi (2012). Geology of the Source Physics Experiment Site, Climax Stock, Nevada National Security Site, *Technical Report DOE/NV/25946--1448*, National Security Technologies, LLC, Las Vegas, Nevada, 442 p.

This page left blank

This page left blank

Sandia National Laboratories

Sandia National Laboratories is a multimission laboratory managed and operated by National Technology & Engineering Solutions of Sandia LLC, a wholly owned subsidiary of Honeywell International Inc. for the U.S. Department of Energy's National Nuclear Security Administration under contract DE-NA0003525.